Physical Science International Journal
14(2): 1-15, 2017; Article no.PSIJ.33042
ISSN: 2348-0130

SCIENCEDOMAIN *international*
www.sciencedomain.org

Structural and Magnetic Properties of Nano Cu-Zn-Zr Ferrite for Magnetic Temperature Transducer (MTT)

O. M. Hemeda[1], M. M. El-Shahawy[1*] and H. E. Khedr[1]

[1]Department of Physics, Faculty of Science, Tanta University, Egypt.

Authors' contributions

This work was carried out in collaboration between all authors. Author OMH designed the study, performed the statistical analysis, wrote the protocol and wrote the first draft of the manuscript. Authors MMES and HEK managed the analyses of the study. Author HEK managed the literature searches. All authors read and approved the final manuscript.

Article Information

DOI: 10.9734/PSIJ/2017/33042
Editor(s):
(1) Yang-Hui He, Professor of Mathematics, City University London, UK and Chang-Jiang Chair Professor in Physics and Qian-Ren Scholar, Nan Kai University, China; & Tutor and Quondam-Socius in Mathematics, Merton College, University of Oxford, UK.
(2) Christian Brosseau, Distinguished Professor, Department of Physics, Université de Bretagne Occidentale, France.
Reviewers:
(1) R. Masrour, Cadi Ayyad University, Morocco.
(2) Birsa Mihail Lucian, Alexandru Ioan Cuza University of Iasi, Romania.
Complete Peer review History: http://www.sciencedomain.org/review-history/18854

Original Research Article

Received 28th March 2017
Accepted 21st April 2017
Published 29th April 2017

ABSTRACT

$Cu_{1-x}Zn_{x+y}Zr_yFe_{2-2y}O_4$ (Cu-Zn-Zr ferrite) series of compositions with x= (zero, 0.4, 0.6, 0.8, 1) when y= (0.05, and 0.1) nanoparticles were synthesized using citrate sol-gel method. The prepared nanoparticles were characterized by X-ray diffraction (XRD) and transmission electron microscopy (TEM). Lattice parameter, bulk density, theoretical density, and porosity were measured for (Cu-Zn-Zr ferrite) samples. The XRD pattern indicated that the average crystallite size found from 18-30 nm and from 17-24 nm, while the average particle size from TEM images are ranging from 21-39 nm and from 18-24 nm for y= (0.05 and 0.1) respectively. Magnetic hysteresis loop measurements illustrate that materials exhibit as soft ferrite properties at low Zn content, while at higher Zn content all materials behave as superparamagnetic materials without any saturation magnetization Ms. The initial magnetic permeability (μ_i) at two frequencies 1 KHz and 10 KHz as a function of temperature was measured. A sudden change in μ_i appear around Curie temperature, making our samples good candidates for Magnetic Temperature Transducer (MTT) devices.

**Corresponding author: E-mail: Mohammed_Elshahawy@science.tanta.edu.eg;*
E-mail: ham_khadr@yahoo.com;

Keywords: Cu-Zn-Zr ferrite, nanoparticles; MTT; XRD; VSM; magnetic hysteresis loop; magnetic properties; magnetic permeability; saturation magnetization; citrate sol-gel method.

1. INTRODUCTION

Over recent decades, nanomaterials represent a great importance because of their unique physical and chemical properties which completely different from their bulk counterparts, and their most important advantage is the miniaturization of particle size. It is known that the preparation method affecting on the effective parameters of ferrites such as magnetization, initial permeability, Curie temperature, and structural properties. Cu-Zn-Zr ferrite nanoparticles possesses important magnetic properties for several advanced technological, industrial, catalytically, and electrical applications e.g. magnetic recording devices, microwave devices, telecommunication equipment, high quality filters, magnetic resonance imaging enhancement, storage devices, power transformers, electric generators…etc. [1-5].

Ferrites have the general formula of $MeFe_2O_4$ (where Me (divalent metallic ion): Fe, Co, Ni, Cu, Mg, etc.,) and a unit cell contains 32 O-atoms in a cubic close packing with 8 (tetrahedral) (A site) and 16 (octahedral) (B site) occupied sites. In most ferrite materials, the substituents play an important role in determining the variation of the physical properties. The substitution can be divided into the following types: direct replacement of Fe^{3+} on tetrahedral (A) or octahedral (B) sub lattice by the substituent ion, with consequential redistribution of Fe^{3+} ions between A and B sub lattices which lead to the change of ferromagnetic spin structure. The extent of iron redistribution depends on the specific nature of the substituting ion. Structural and magnetic properties of spinel ferrites $MeFe_2O_4$ strongly depend upon the nature, concentration, and distribution of the substituted Me cations on A and B sites as well as the method of preparation and characterization [6-8].

By virtue of their magnetic and semiconducting properties, the copper ferrites and its compositions with other ferrites are employed as magnetic materials for multiplayer chip inductors but also for transducers of high thermo-magnetic sensitivity [9]. Currently, a new type of temperature-sensitive element using for construction of devices for controlling temperature. The sudden change of initial magnetic permeability near Curie temperature represent the main factor to using such element [3]. Many researchers was reported the substitution of different elements such as Co [10], Ni [11-13] and Tb [14] in ferrites to enhance their magnetic and electrical properties [15].

Presently, various physical and chemical techniques have been developed to prepare nanomaterials. The chemical techniques for the synthesis of nanostructured materials offer some advantages in comparison with the physical techniques in relation to simplicity, energy saving and product homogeneity[6]. The widely used chemical methods are co-precipitation [16], hydrothermal [17], electro deposition [18], micro-emulsion [19], auto-combustion [20], sucrose method [21], reverse micelle [22],and Citrate Sol-Gel technique [23,24].

Among these methods, the citrate-gel method can be used to prepare nanocomposite of spinel ferrites with specific properties, such as controlled stoichiometry and narrow particle size distribution. The cheapness, simplicity of experimental set-up, short time of production and the purity and homogeneity of final product are the most important features that distinguish this technique. In addition, the speed and low temperature of the synthesis process prevent the sintering of the obtained samples; which confirms that this technique is special compared with other synthesis techniques [25].

This paper aims to study the substitution influence of Zn and Zr on structure, microstructure, and consequently, magnetic properties of Cu ferrite.

2. EXPERIMENTAL

2.1 Materials

The starting materials for the citrate precursor synthesis route were $Cu(NO_3)_2.3H_2O$, $Fe_2(NO_3)_3.9H_2O$, $Zn(NO_3)_2.6H_2O$, $ZrOCl_2.8H_2O$ and citric acid ($C_6H_8O_7$) were of analytical grade.

2.2 Synthesis of Cu-Zn-Zr Nano Ferrites

The samples were prepared by sol-gel method and was annealed at 800℃. The first step is the formation of complex compounds (chelates) between polybasic citric acid and various metal cations. In typical procedure, the stoichiometric amounts of cupper nitrate, ferric nitrate, zinc nitrate, and zirconium oxychloride were taken in a glass beaker and dissolved in de-ionized water.

The compositions of the Zn and Zr-substituted $CuFe_2O_4$ were represented by $Cu_{1-x}Zn_{x+y}Zr_yFe_{2-2y}O_4$ with x= (zero, 0.4, 0.6, 0.8, 1) when y= (0.05, and 0.1). The solution was heated on a hot plate up to 60℃ then citric acid was added. The metal nitrates: citric acid molar ratio was fixed at 1:1. The citrate–nitrate mixture was heated and vigorously stirred with magnetic stir bar at 90℃ until a gel was formed. The resulting gel was placed in a drying oven at 105℃ for 24 hours. The dried gel was crushed using an agate mortar and transformed into muffle furnace then fired at 800℃ in alumina crucibles.

2.3 Characterization of Cu-Zn-Zr Nano Ferrites

The X-ray diffraction (XRD) of nano ferrite was carried out at room temperature using (APD 2000 pro, H423-virtical diffractometer) equipped with Cu Kα radiation (λ = 1.540598 Å). The crystallite size of the samples were investigated by JEOL JEM-2100 transmission electron microscopy (TEM). The TEM specimen was prepared by the ultrasonic dispersion of small amount of the powders in a few milliliters of ethanol, and then dropping on a copper grid covered in an amorphous carbon film. The initial permeability (μ_i) was measured using (MCH2811C digital bridge) at two frequencies 1KHz and 10KHz as a function of temperature for different Zn and Zr contents. The magnetic measurements were carried out at room temperature using vibration sample magnetometer (VSM) operating system v 1.6 control software Oxford OX8JTL England.

3. RESULTS AND DISCUSSION

3.1 X-Ray Diffraction Studies

Fig. 1. (a) and (b) shows the X-Ray diffraction patterns of Cu-Zn ferrite doped with Zr ions with mole content 0.05 and 0.1 respectively. The diffraction patterns confirm the formation of single-phase spinel structure without presence of foreign peaks especially at high Zn content. At low value of Zn content, some peaks belong to other phases are present which disappear at high Zn content. This indicates the role that Zn ion plays as a catalyst for speeding the solid-state reaction and the formation of single phase. The particle size was calculated from the most intense peaks [(220) (311) (511) (440)] by using Scherer's equation [26,27]:

$$D = \frac{K\lambda}{\beta \cos\theta}$$

Where K is the Scherer's constant and equal 0.89. The value of K depends on several factors including the Miller indices of the reflection plane and the shape of phase crystal. If the shape is unknown K often assigned of 0.89, λ is the wavelength of the X-ray for Cu-Kα (λ =1.540598$\AA$), θ is the diffraction angle and β is the full width at half maximum (FWHM) in radian.

Table 1 shows that the crystallite size (D) decrease for both series (y=0.05 and 0.1) above x=0.4 by increasing Zn^{2+} contents then increase at x=1. The value of lattice constant (a) increase by increasing Zn contents for Zr^{4+} ion = 0.05 and 0.1. When a cation whose radius and valance are differ from those of the host cations is introduced into the spinel lattice, a strain in the lattice is created which affect the unit cell dimensions.

The ionic radii of Zn^{2+} ions 0.74($\AA$) and Zr^{4+} ions 0.79($\AA$) are larger than that of Fe^{3+}ions 0.64($\AA$), the lattice seems to expand likely to accommodate the increasing number of Zn^{2+} and Zr^{4+} ions resulting into the increasing of lattice constant.

Table 1. The structural parameters of (Cu-Zn-Zr) ferrite samples

y	x	Lattice parameters		Particle size D (nm) from X-ray	Cell volume V_{exp} $(\AA)^3$	Particle size D (nm) from TEM	(d) nm	Plane
		a_{th} ($\AA$)	a_{exp} ($\AA$)					
0.05	0	8.37	8.39	29.9	590.6	——	——	——
	0.4	8.39	8.44	30.2	601.2	36.98	——	——
	0.6	8.4	8.50	20.8	614.1	33.22	0.29	(220)
	0.8	8.41	8.51	18.7	616.3	——	——	——
	1	8.41	8.44	23.2	601.2	——	——	——
0.1	0	8.39	8.39	19.4	590.6	——	——	——
	0.4	8.41	8.41	24.1	594.8	28.06	0.27	(311)
	0.6	8.42	8.42	17.6	596.9	23.81	0.22	(400)
	0.8	8.426	8.43	17.6	599.1	——	——	——
	1	8.431	8.46	19.7	605.5	——	——	——

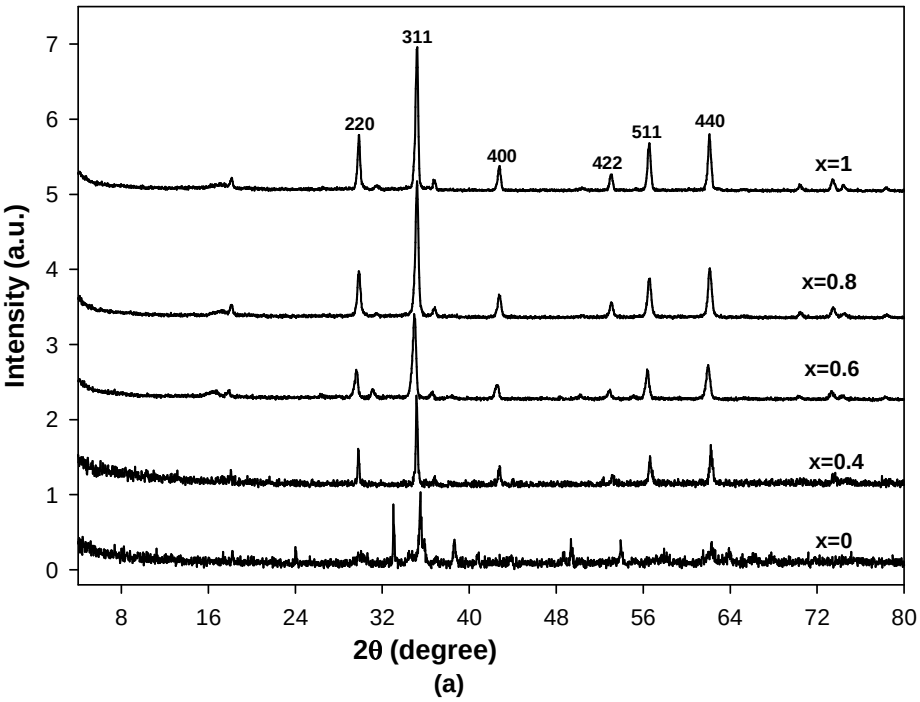

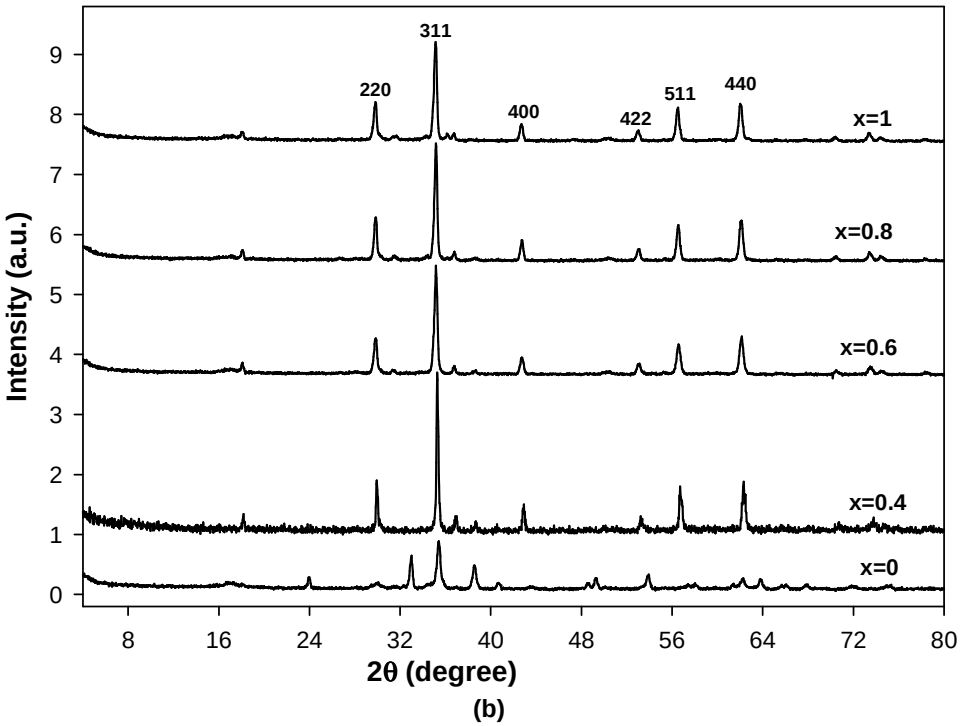

Fig. 1. The XRD patterns of the prepared $Cu_{1-x}Zn_{x+y}Zr_yFe_{2-2y}O_4$ where x= (zero, 0.4, 0.6, 0.8, 1), (a) y=0.05, and (b) y= 0.1

The measured experimental density was calculated from Archimedes principle and are shown in Fig. 2. From this figure it is evident that, the measured density increase with Zn and Zr contents in the lattice which may be attributed to the difference of atomic weights of Zn^{2+} , $Zr^{4+}$and Fe^{3+}. The presence of Zn ions enhance the grain growth due to the great solubility in the spinel phase at higher concentration.

The theoretical density of spinel phase were calculated from the following equation [28]:

$$D_x = \frac{8M}{Na^3} \text{ (g/cm}^3\text{)}$$

Where M is the molecular weight, N is the Avogadro's number, equal to (6.022×10^{23} mole^{-1}).

The theoretical density nearly remain constant by increasing Zn contents and has larger value than bulk density due to the presence of pores in the material. The X-ray density increase with increasing Zn and Zr contents, which is referred to the increase in atomic weight while the porosity of the samples decrease with increasing Zn and Zr contents as shown in Fig. 2.

Fig. 3. show the relation between the radius of tetrahedral (A-Site) and octahedral (B-Site) respectively as a function of Zn content. The radius of tetrahedral site r_A decrease by increasing the Zn contents while the radius of octahedral site r_B increase. The substitution of Zn^{2+} ions with radius 0.74$\AA$ instead of Fe^{3+} ions leads to increase of r_A. The decrease of cation with radius 0.72$\AA$ at octahedral site leads to the decrease of r_B. The addition of Zr^{4+} ions does not affect on the r_B due to its small ratio.

The expected cation distribution of our samples may be given from the following formula:

$$(Zn_{x+y}\ Zr_{y-t}\ Fe_{1-x-2y+t}\ )[Cu_{1-x}\ Zr_t\ Fe_{1+x-t}\ ],\quad t = 0.2y$$

The theoretical lattice parameter can be calculated using the value of r_A, r_B and R_O(radius of oxygen ion) from the following relation [29]:

$$a = \frac{8}{3\sqrt{3}}[(r_A + R_O) + \sqrt{3}(r_B + R_O)]\ (\AA)$$

To calculate r_A and r_B, it is necessary to know the cation distribution which can represented by the above estimated equation at which the theoretical and experimental lattice parameter are co-inside. The expected cation distribution are given in Table 2.

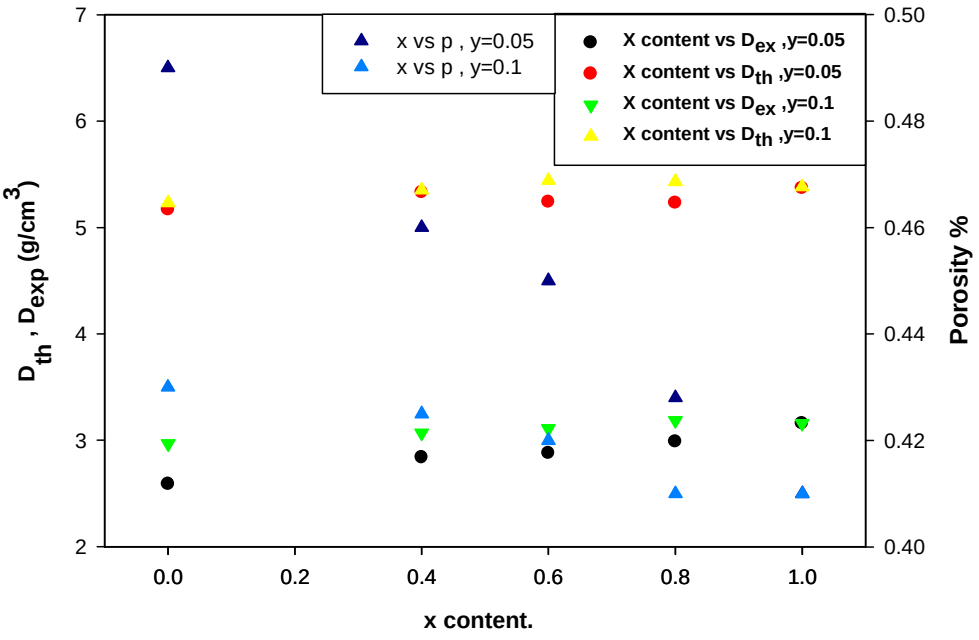

Fig. 2. The porosity, theoretical density and bulk density with x content for prepared samples

Table 2. Cation distribution for (Cu-Zn-Zr) ferrite samples

y	x	Chemical structure	A-Site	B-Site
0.05	0	$Cu_1Zn_{0.05}Zr_{0.05}Fe_{1.9}O_4$	$(Zn_{0.05}Zr_{0.04}Fe_{0.91})$	$[\boldsymbol{Cu_1Zr_{0.01}Fe_{0.99}}]$
	0.4	$Cu_{0.6}Zn_{0.45}Zr_{0.05}Fe_{1.9}O_4$	$(Zn_{0.45}Zr_{0.04}Fe_{0.51})$	$[\boldsymbol{Cu_{0.6}Zr_{0.01}Fe_{1.39}}]$
	0.6	$Cu_{0.4}Zn_{0.65}Zr_{0.05}Fe_{1.9}O_4$	$(Zn_{0.65}Zr_{0.04}Fe_{0.31})$	$[\boldsymbol{Cu_{0.4}Zr_{0.01}Fe_{1.59}}]$
	0.8	$Cu_{0.2}Zn_{0.85}Zr_{0.05}Fe_{1.9}O_4]$	$(Zn_{0.85}Zr_{0.04}Fe_{0.11})$	$[\boldsymbol{Cu_{0.2}Zr_{0.01}Fe_{1.79}}]$
	1	$Cu_0Zn_{1.05}Zr_{0.05}Fe_{1.9}O_4$	(Zn_1)	$[\boldsymbol{Zn_{0.05}Zr_{0.05}Fe_{1.9}}]$
0.1	0	$Cu_1Zn_{0.1}Zr_{0.1}Fe_{1.8}O_4$	$(Zn_{0.1}Zr_{0.08}Fe_{0.82})$	$[\boldsymbol{Cu_1Zr_{0.02}Fe_{0.98}}]$
	0.4	$Cu_{0.6}Zn_{0.5}Zr_{0.1}Fe_{1.8}O_4$	$(Zn_{0.5}Zr_{0.08}Fe_{0.42})$	$[\boldsymbol{Cu_{0.6}Zr_{0.02}Fe_{1.38}}]$
	0.6	$Cu_{0.4}Zn_{0.7}Zr_{0.1}Fe_{1.8}O_4$	$(Zn_{0.7}Zr_{0.08}Fe_{0.22})$	$[\boldsymbol{Cu_{0.4}Zr_{0.02}Fe_{1.58}}]$
	0.8	$Cu_{0.2}Zn_{0.9}Zr_{0.1}Fe_{1.8}O_4$	$(Zn_{0.9}Zr_{0.08}Fe_{0.02})$	$[\boldsymbol{Cu_{0.2}Zr_{0.02}Fe_{1.78}}]$
	1	$Cu_0Zn_{1.1}Zr_{0.1}Fe_{1.8}O_4$	(Zn_1)	$[\boldsymbol{Zn_{0.1}Zr_{0.1}Fe_{1.8}}]$

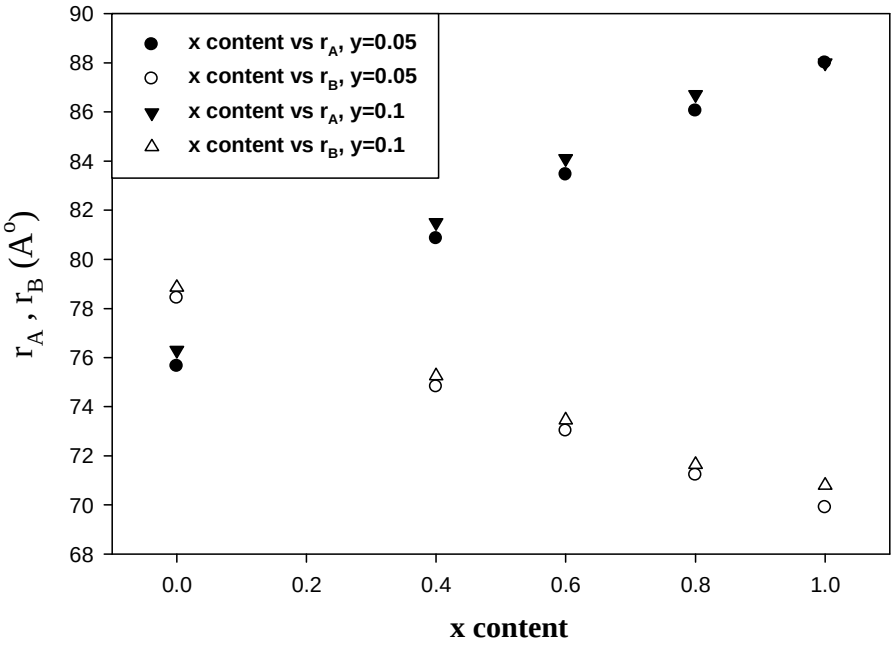

Fig. 3. The radius of tetrahedral (A-Site) and octahedral (B-Site) for our samples

3.2 The Transmission Electron Microscopy (TEM)

The high resolution transmission electron microscope (HRTEM) was employed to confirm the results of XRD studies. Fig. 4. (a) and (b) shows the high crystallinity nature of the synthesized $Cu_{1-x}Zn_{x+y}Zr_yFe_{2-2y}O_4$ nanoparticles at (x=0.4 and 0.6) for both ratios of (y=0.05 and 0.1). The nanoparticles exhibit a cubic shapes where their diameter ranging from 17-39 nm with decreasing value by increasing Zn and Zr contents. The crystallite size deduced from TEM were near to that calculated from XRD as shown in Table 1. The lattice planes and its spacing appear clearly from the HRTEM which confirm the crystalline nature of the samples. The interplanner distance (d) was found to be 0.27 nm for x=0.4, y=0.1 which belong (311) plane. Other values of d spacing was 0.29 nm for x=0.6, y=0.05 which belong to (220) plane and 0.22 nm for x=0.6, y=0.1 that belong to (400) plane.

3.3 Initial Magnetic Permeability

The initial permeability (μ_i) was measured at two frequencies 1 KHz and 10KHz as a function of temperature for different Zn and Zr contents which are shown in Fig. 5.

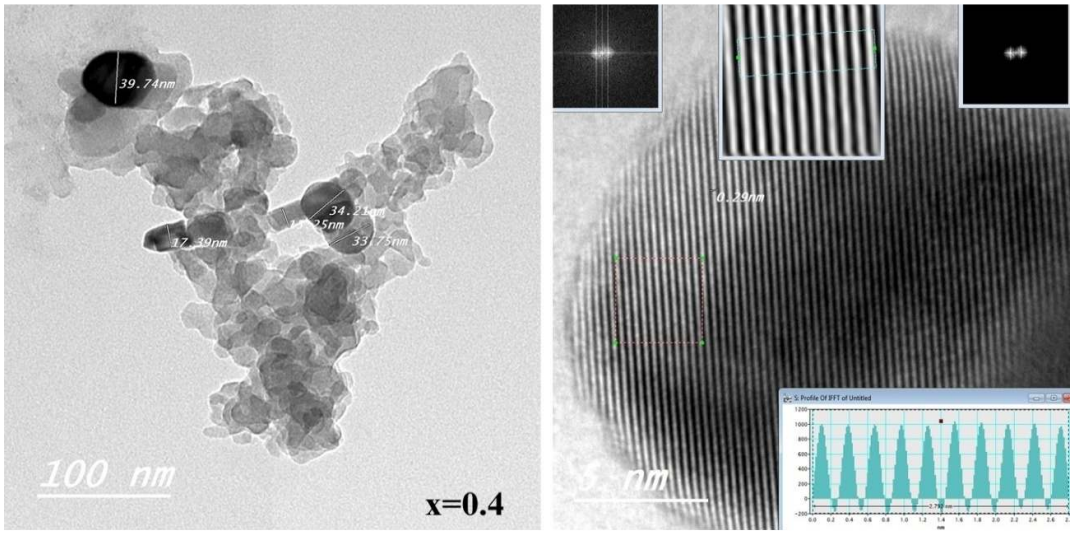

(a)

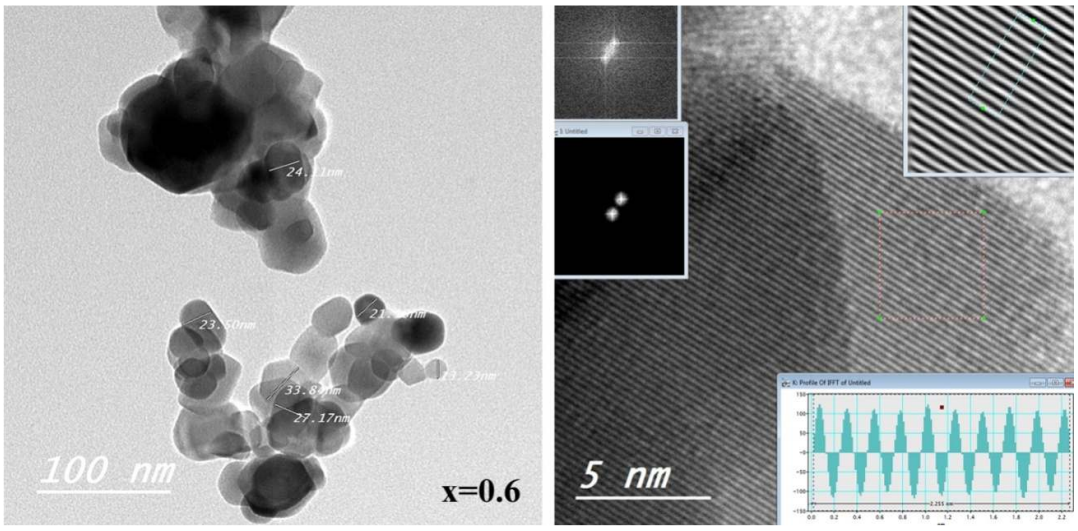

(b)

Fig. 4. (a) and (b) The TEM and (HRTEM) images of $Cu_{0.6}Zn_{0.5}Zr_{0.1}Fe_{1.8}O_4$ and $Cu_{0.4}Zn_{0.7}Zr_{0.1}Fe_{1.8}O_4$ samples respectively

The permeability at room temperature as a function of Zn and Zr contents is shown in Fig. 6. for both Zr ratios 0.05 and 0.1.

The increase of μ_i as Zn content increase up to x=0.4 is attributed to the decrease in magnetic anisotropy field according to Globus relation [30]:

$$\mu_i = \frac{M_S^2 D}{\sqrt{K}}$$

where K is anisotropy constant, D is the average grain size and M_s is the saturation magnetization.

About x=0.4, the permeability decrease due to the decrease of saturation magnetization M_s. The two compotation factors affect the permeability are the magnetic anisotropy and saturation magnetization.

Noticeable hump appear in all samples near Curie temperature which indicate the presence of single phase structure. After the hump, the μ_i decrease sharply and reach to very small value near zero due to the transformation from ferromagnetic to paramagnetic. The presence of hump is due to the fast decrease in magnetic

anisotropy than the saturation magnetization. The fast decrease in initial permeability μ_i at T_c is a good reason to be a very strong candidate for magnetic switch devices.

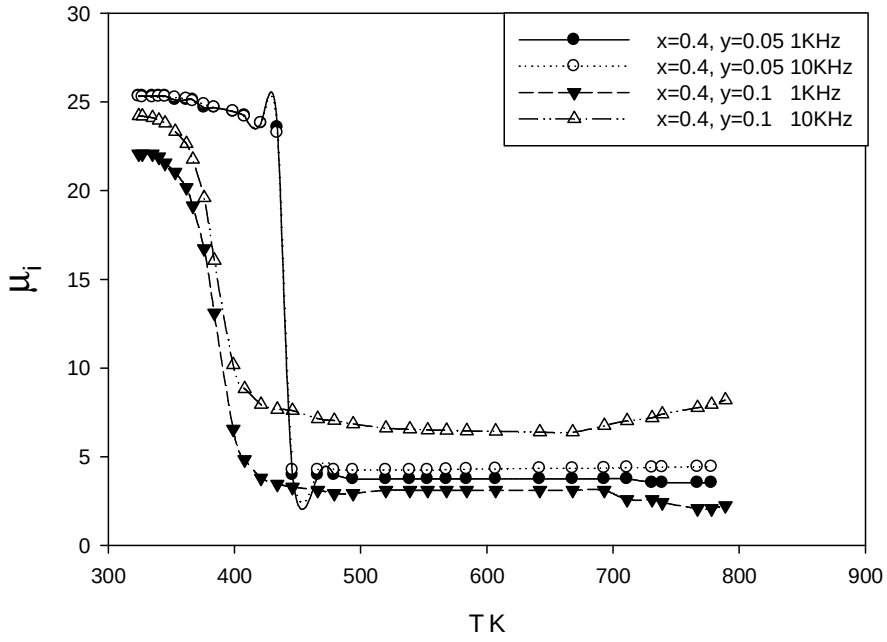

(a)

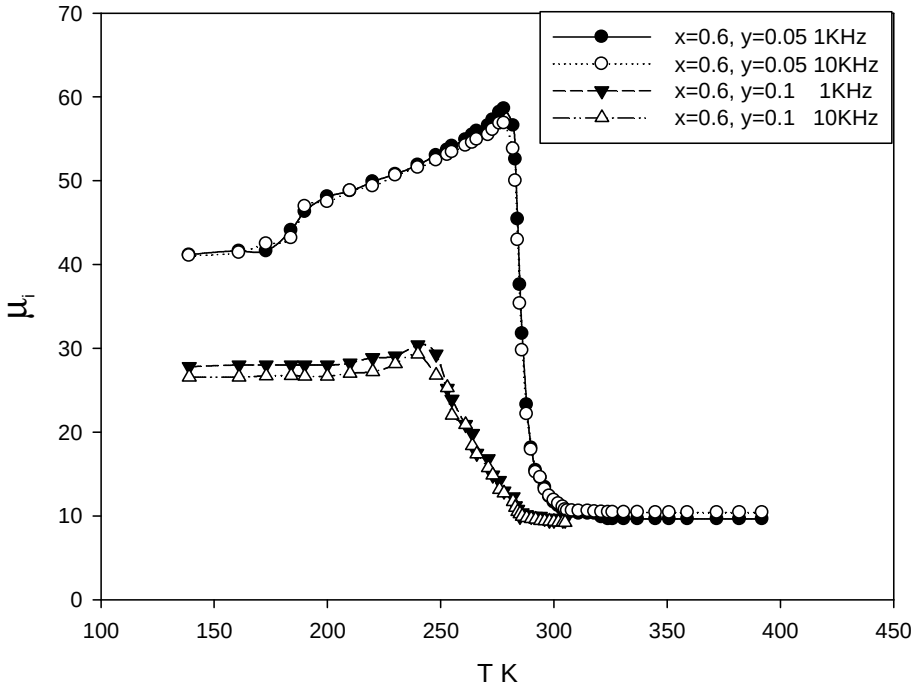

(b)

Fig. 5. The variation of initial magnetic permeability (μ_i) with temperature at two frequencies

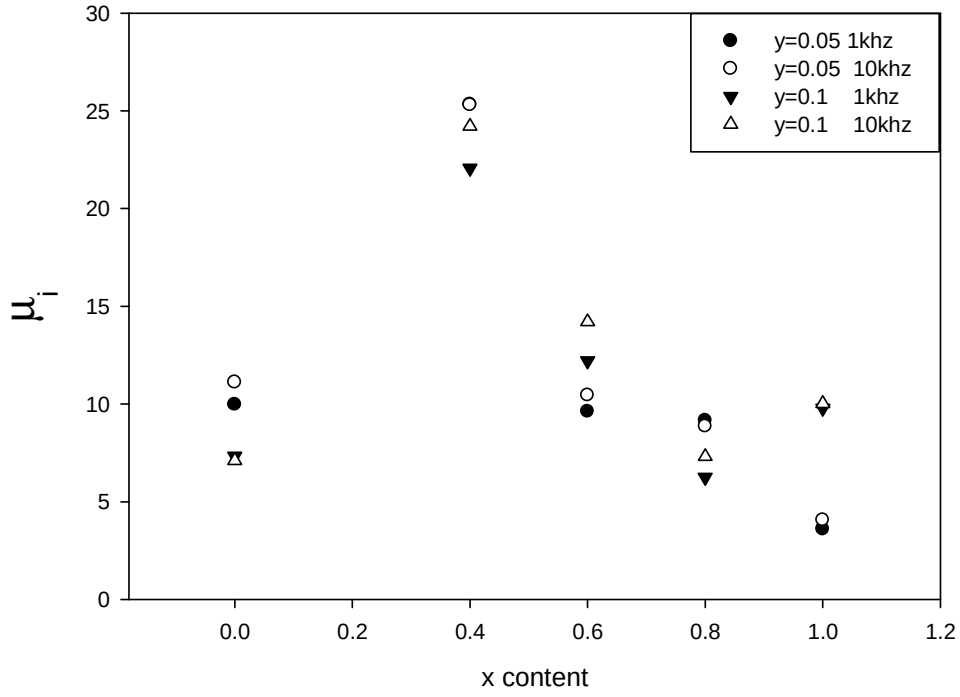

Fig. 6. The variation of magnetic permeability (μi) with x content for both series at two frequencies

The Curie temperature decrease by increasing Zn contents up to x=0.6 for both ratios of y (0.05 and 0.1) and then increase. It seems to have an opposite relation with saturation magnetization. The Curie temperature obtained from permeability are given in Table 3. Furthermore it is obvious that, the μ_i at low Zn content has an inverse relation with the porosity which insure that, the porosity affect and decrease the domain wall motion which consider as the origin of magnetic permeability.

The Curie temperature was determined from the interception of extrapolation of linear part of permeability with temperature axes. The value of T_c and the temperature rate of change of permeability (slope of linear part) are given in Table 3. We can conclude that, the presence of Zn increase the permeability and decrease the Curie temperature, that we can obtain magnetic material with the desired Curie temperature by simply controlling Zn content in $CuFe_2O_4$. This material called magnetic temperature transducer, which have a sudden change in permeability. The higher the slope, the better the devise for controlling temperature.

Table 3. The values of T_c (K) and rate of decrease μ_i with x content

y	x	T_c (K)		Rate of decrease μ_i (K^{-1})	
		1KHz	10KHz	1KHz	10KHz
0.05	0	773	773	-0.18	-0.15
	0.4	456	456	-0.63	0.61
	0.6	278	278	-7.02	-6.83
	0.8	533	——	-0.007	——
	1	720	——	-0.18	——
0.1	0	724	735	-0.14	-0.19
	0.4	340	340	-0.35	-0.32
	0.6	224	224	-0.62	0.58
	0.8	544	——	-0.01	——
	1	683	——	-0.14	——

Moreover, it was found that, the presence of Zr gives rise to further decrease in permeability and Curie temperature, which make this material very sensitive to thermal change. The decrease in Curie temperature may be due to the decrease in A-B exchange interaction, which reduce the magnetization and consequently Curie temperature.

From the above discussion, we can say that our samples are suitable for magnetic temperature sensors and devices for temperature controller or it act as (MTT).

3.4 Low Field Hysteresis Loop

Fig. 7. shows the magnetic hysteresis loop for $CuFe_2O_4$ doped with Zn at different ratios of Zr (0.05 and 0.1). The material exhibit typical magnetic hysteresis loop of soft ferrite which indicate that, it is magnetically ordered at low Zn content. At higher Zn content (x=0.6, 0.8 and 1) the material behave as super paramagnetic material without any saturation M_s and very small coercivity around zero. This behavior is attributed to the very small crystalline size (around 25 nm) at this range. The canting effect at octahedral sites, which arrange the magnetic moments in different directions and not parallel may be the reason for this behavior.

The dependence of saturation magnetization on Zn and Zr contents are illustrated in Fig. 8. It was found that, M_s increases up to x=0.4 and then decrease which mean that, there is a limit for the material in ferrimagnetic region and after this limit (x=0.4) the material transfer to super paramagnetic behavior. It is clearly observed that, M_s increases up to x=0.4 according to the resultant sub lattice magnetic moment in the basis of Neel's theory model [31].

The theoretical magnetic moment μ_{th} is given by μ_{th} = |M| = $|M_B|$– $|M_A|$. The μ_{th} depends on the A and B cation distribution which estimated from X-Ray analysis as given before. The general formula for μ_{th} is given by:

μ_{th}=[1.73(1-x)+5(2x+y)]μ_B for low Zn content.

μ_{th}=[1.73(1-x)+5(2x+y-2t)]μ_B for high Zn content.

Where t=0.2y and μ_B is Bohr magneton.

The magnetic moment depends on the cation distribution among the two sites A and B taking into account that, Zn and Zr are not magnetic materials. The replacement of high spin magnetic moment ions as Fe^{3+} (5 μ_B) and Cu^{2+} (1.73 μ_B) by a non magnetic ions Zn^{2+} and Zr^{4+} leads to the weakening of the A and B exchange interaction which is responsible for the decrease of M_s at high Zn contents. The experimental magnetic moment can be calculated from the relation [32]:

$$\mu_{exp} = \frac{M_{w}.M_S}{5585}$$

Where M_s is the saturation magnetization obtained from hysteresis loop curve.

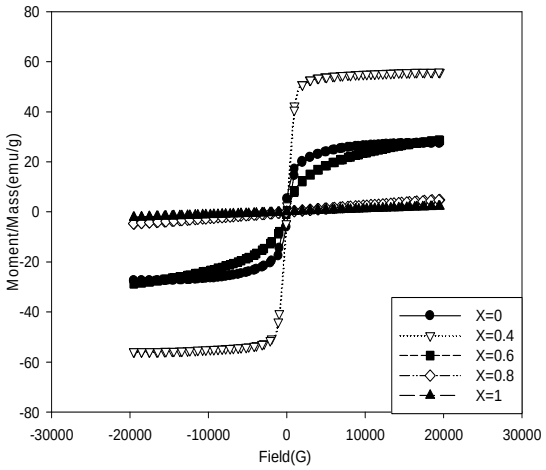

(a)

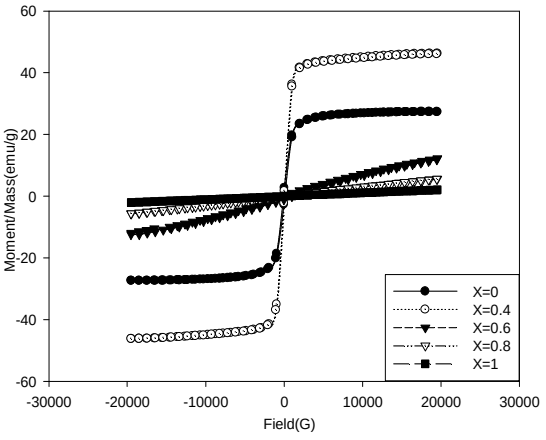

(b)

Fig. 7. Magnetic hysteresis loop for Cu Zn Zr Ferrite when (a) y=0.05 and (b) y=0.1

The canting at B site means disturbance of the parallel arrangement of spin magnetic moment. The presence of canting spin gives rise to the

Yafet-Kittel angle. The Yafet-Kittel angle has been calculated at room temperature using the formula [32]:

$$\mu_{exp} = \mu_B COS\alpha_{Y-K} - \mu_A$$

Where α_{Y-K} is the Yafet-Kittel anglethat calculate the strength of A-B and B-B exchange interaction.

The values of μ_{th} , μ_{exp} and α_{Y-K} for the samples were measured at room temperature are given in Table 4. The μ_{exp} decrease above x=0.4 indicating the probability of non collinear spin at A-Site which is due to the canting between of spin moment.

To show the effect of nanostructure on the magnetic properties, a correlation between the crystalline size and saturation magnetization for both ratios was done, and is shown in Fig. 9. It was observed that, the average crystalline size increases up to x=0.4 and then decrease further. This variation follow nearly the same trend of M_s and μ_{exp} . Similar results has been reported by [33].

The large ionic radius of Zr^{4+} increase the separation between Fe^{3+} ions at B site. Such displacement between Fe^{3+} ions decrease the B-B exchange interaction leading to the decrease of M_s at high Zn and Zr contents. The corecivity of the studied samples which can be estimated from H-Loop has high values at low Zn content compared with the very low values at high Zn content, which is an indicator to the super paramagnetic behavior of the material.

Table 4. Experimental and theoretical magnetic moments for y=0.05 and 0.1

y	x	$\mu_{th}(\mu_B)$	$\mu_{exp}(\mu_B)$	α_{Y-K}
0.05	0	1.98	1.18	120
	0.4	5.28	2.42	90.9
	0.6	6.84	1.24	92
	0.8	8.49	0.20	92.1
	1	10.15	0.09	89.4
0.1	0	2.23	1.19	116
	0.4	5.53	1.98	90.8
	0.6	6.99	0.54	93.7
	0.8	10.2	0.24	89.1
	1	10.3	0.09	89.4

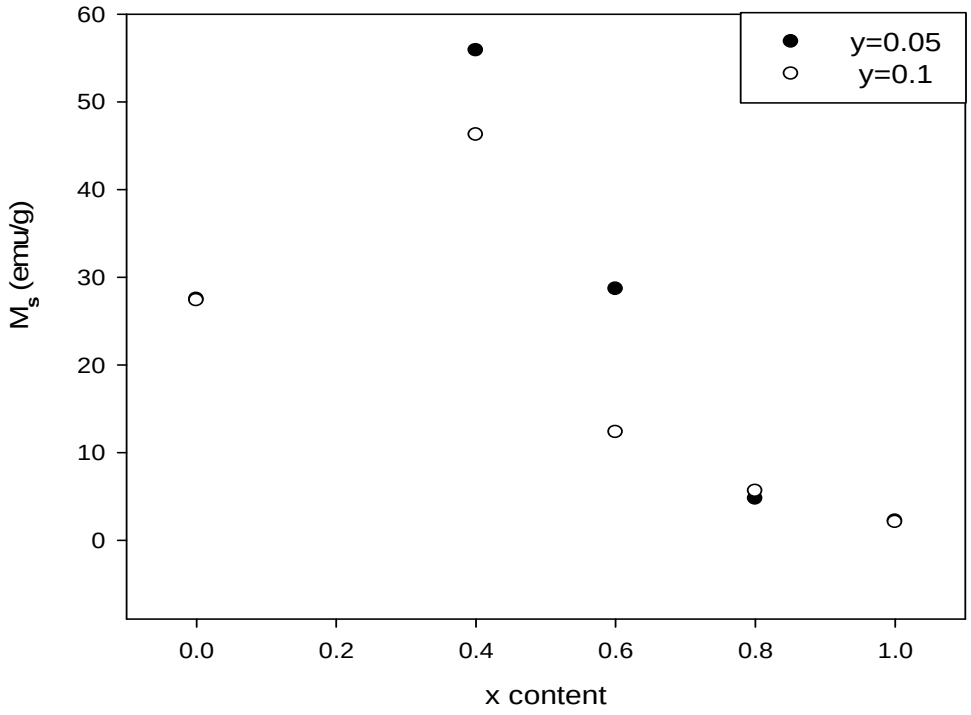

Fig. 8. The variation of M_s with x content for both series

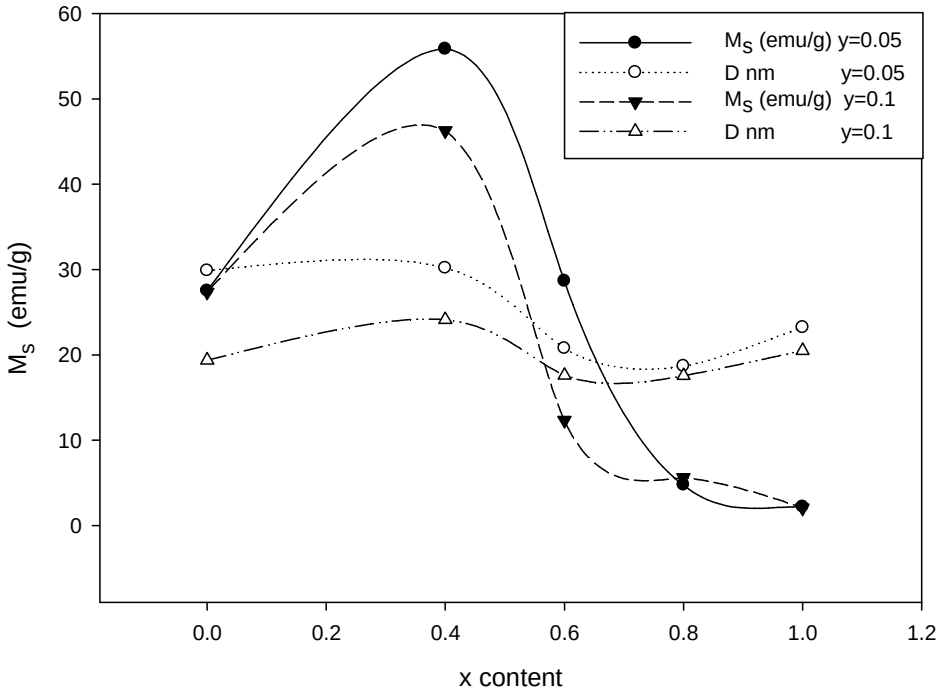

Fig. 9. The variation of crystalline size and saturation magnetization with x content for both ratios

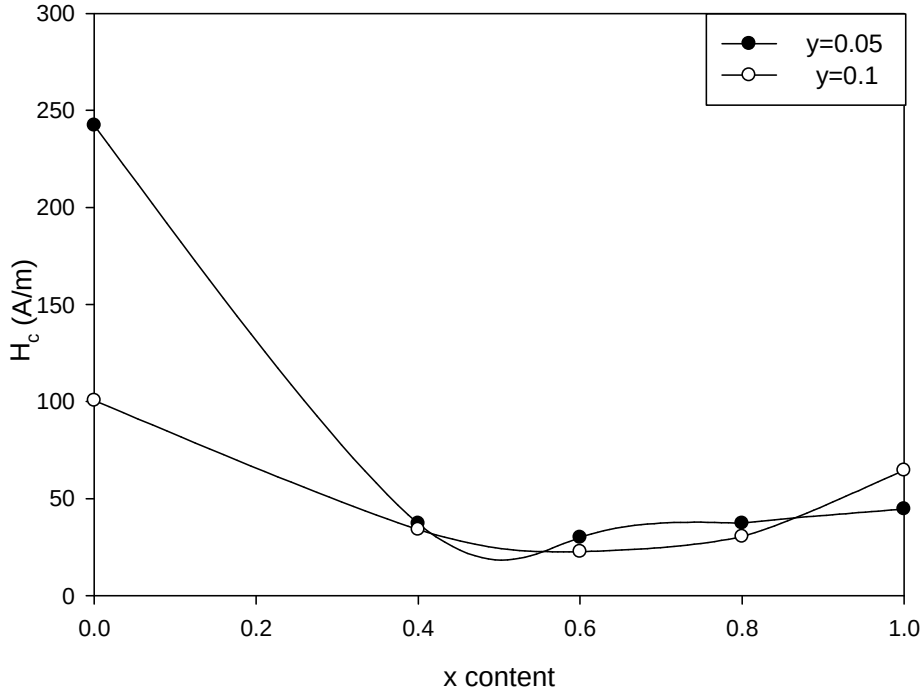

Fig. 10. The variation of coercivity with x content for both ratios

Fig. 10. shows the decrease in H_c with the increase in Zn and Zr contents due to the decrease of magnetic crystalline anisotropy [34] according to Brown's relation [30]:

$$H_c \geq \frac{2\,k_i}{\mu_\circ M_s}$$

Where k is the magnetic anisotropy and $\mu_\circ$ is the universal constant of permeability for free space.

It is evident that H_c decreases by increasing Zn contents while the permeability increase and has highest value at x= 0.4 (Zn content = 0.45 at y=0.05 and 0.5 at y=0.1). This behavior can be explained by the previous relation which means that, there is a relation between initial permeability μ_i and coercivity H_c according to Globus relation [30].

$$\mu_i = \frac{M_s^2 D}{\sqrt{k}}$$

With the increase of Zn content, the formation probability of Fe^{2+} decrease which is the responsible reason for the decrease of anisotropy and leads to the increase of permeability.

When the permeability decrease, the coercivity still decrease also which indicates that, the anisotropy constant K is the dominant factor in this range up to x=0.4. The same behavior was observed in the previous study [35,36].

4. CONCLUSIONS

Copper Ferrite nanoparticles have been prepared by citrate sol gel technique. X-ray diffraction pattern confirm the formation of single phase structure. The crystallite size from TEM micrograph and XRD ranged from (17.5-37) nm. Lattice parameter was found to increase by increasing Zn and Zr contents. Initial permeability remains constant with temperature and suddenly drops to near zero at certain temperature called curie temperature which indicates the formation of single phase of the compounds. The initial permeability has maximum value at x=0.4. The T_c show decreasing trend by increasing Zn and Zr contents. Low field hysteresis loop indicates that, the materials were magnetically ordered at low Zn content up to x=0.4. After that, the materials behave as a super paramagnetic without any M_s and very small coercivity H_c around zero.

COMPETING INTERESTS

Authors have declared that no competing interests exist.

REFERENCES

1. Hassan A, Khan MA, Shahid M, Asghar M, Shakir I, Naseem S, Riaz S, Warsi MF. Nanocrystalline Zn 1− x Co 0.5 x Ni 0.5 x Fe 2 O 4 ferrites: Fabrication via co-precipitation route with enhanced magnetic and electrical properties. Journal of Magnetism and Magnetic Materials. 2015; 393:56-61.
2. Sattar A, El-Sayed H, Agami W, Ghani A. Magnetic properties and electrical resistivity of Zr $^{4+} $ substituted Li-Zn ferrite. Amer J Appl Sci. 2007;4:89-93.
3. Mahmoud K, Hemeda O. Structural, magnetic, and positron annihilation characteristics of Zn and Zr-substituted CuFe2O4 for magnetic temperature controller. Journal of Superconductivity and Novel Magnetism. 2016;29(10):2669-2679.
4. Rashad M, Mohamed R, Ibrahim M, Ismail L, Abdel-Aal E. Magnetic and catalytic properties of cubic copper ferrite nanopowders synthesized from secondary resources. Advanced Powder Technology. 2012;23(3):315-323.
5. Masrour R, Hamedoun M, Benyoussef A, Hlil E. Magnetic properties of mixed Ni–Cu ferrites calculated using mean field approach. Journal of Magnetism and Magnetic Materials. 2014;363:1-5.
6. Sridhar R, Dachepalli R, K. Vijaya K. Synthesis and characterization of copper substituted nickel nano-ferrites by citrate-gel technique. Advances in Materials Physics and Chemistry; 2012.
7. Roy P, Nayak BB, Bera J. Study on electro-magnetic properties of La substituted Ni–Cu–Zn ferrite synthesized by auto-combustion method. Journal of Magnetism and Magnetic Materials. 2008; 320(6):1128-1132.
8. El Moussaoui H, Masrour R, Mounkachi O, Hamedoun M, Benyoussef A. Cation distribution and magnetic interactions in Zn-substituted Fe (Cu) Fe2O4 ferrites. Journal of superconductivity and Novel Magnetism. 2012;25(7):2473-2480.
9. Miclea C, Tanasoiu C, Miclea CF, Spanulescu I, Cioangher M, Miclea CT. Magnetic temperature transducers made

from copper based soft ferrite. Smart Materials & Micro/Nanosystems. 2009; 54:62-69.
10. Malik H, Mahmood A, Mahmood K, Lodhi MY, Warsi MF, Shakir I, Wahab H, Asghar M, Khan MA. Influence of cobalt substitution on the magnetic properties of zinc nanocrystals synthesized via micro-emulsion route. Ceramics International. 2014;40(7):9439-9444.
11. Rashad M, Elsayed E, Moharam M, Abou-Shahba R, Saba A. Structure and magnetic properties of Ni x Zn 1− x Fe 2 O 4 nanoparticles prepared through co-precipitation method. Journal of Alloys and Compounds. 2009;486(1):759-767.
12. Priyadharsini P, Pradeep A, Rao PS, Chandrasekaran G. Structural, spectroscopic and magnetic study of nanocrystalline Ni–Zn ferrites. Materials Chemistry and Physics. 2009;116(1):207-213.
13. Shahane G, Kumar A, Arora M, Pant R, Lal K. Synthesis and characterization of Ni–Zn ferrite nanoparticles. Journal of Magnetism and Magnetic Materials. 2010; 322(8):1015-1019.
14. Khan MA, Sabir M, Mahmood A, Asghar M, Mahmood K, Khan MA, Ahmad I, Sher M, Warsi MF. High frequency dielectric response and magnetic studies of Zn 1− x Tb x Fe 2 O 4 nanocrystalline ferrites synthesized via micro-emulsion technique. Journal of Magnetism and Magnetic Materials. 2014;360:188-192.
15. Haque MM, Huq M, Hakim M. Influence of CuO and sintering temperature on the microstructure and magnetic properties of Mg–Cu–Zn ferrites. Journal of Magnetism and Magnetic Materials. 2008; 320(21):2792-2799.
16. Kannan Y, Saravanan R, Srinivasan N, Praveena K, Sadhana K. Synthesis and characterization of some ferrite nanoparticles prepared by co-precipitation method. Journal of Materials Science: Materials in Electronics. 2016; 27(11):12000-12008.
17. Xia A, Zuo C, Chen L, Jin C, Lv Y. Hexagonal SrFe 12 O 19 ferrites: Hydrothermal synthesis and their sintering properties. Journal of Magnetism and Magnetic Materials. 2013;332:186-191.
18. Erb U. Electrodeposited nanocrystals: Synthesis, properties and industrial applications. Nanostructured Materials. 1995;6(5):533-538.
19. O'Connor CJ, Kolesnichenko V, Carpenter E, Sangregorio C, Zhou W, Kumbhar A, Sims J, Agnoli F. Fabrication and properties of magnetic particles with nanometer dimensions. Synthetic Metals. 2001;122(3):547-557.
20. Liu T, Wang L, Yang P, Hu B. Preparation of nanometer CuFe 2 O 4 by auto-combustion and its catalytic activity on the thermal decomposition of ammonium perchlorate. Materials Letters. 2008; 62(24):4056-4058.
21. Das R. Nanocrystalline ceramics from sucrose process. Materials Letters. 2001; 47(6):344-350.
22. Gubbala S, Nathani H, Koizol K, Misra R. Magnetic properties of nanocrystalline Ni–Zn, Zn–Mn, and Ni–Mn ferrites synthesized by reverse micelle technique. Physica B: Condensed Matter. 2004; 348(1):317-328.
23. Chang S. Fabrication of m-type barium ferrite nano-powder with citrate sol-gel precess. IJSTR. 2015;4(10):110-112.
24. Yu F, Yuan D, Duan X, Kong L, Shi X, Guo S, Wang L, Cheng X, Wang X. Citrate sol–gel method to prepare nanoparticles of a piezoelectric crystal material: La 3 Nb 0.5 Ga 5.5 O 14 at low temperature. Journal of Alloys and Compounds. 2008;459(1):L1-L4.
25. Zahi S, Daud AR, Hashim M. A comparative study of nickel–zinc ferrites by sol–gel route and solid-state reaction. Materials Chemistry and Physics. 2007; 106(2):452-456.
26. Bahgat M, Farghaly F, Basir SA, Fouad O. Synthesis, characterization and magnetic properties of microcrystalline lithium cobalt ferrite from spent lithium-ion batteries. Journal of Materials Processing Technology. 2007;183(1):117-121.
27. El Moussaoui H, Mahfoud T, Ali MB, Mahhouti Z, Masrour R, Hamedoun M, Hlil E, Benyoussef A. Experimental studies of neodymium ferrites doped with three different transition metals. Materials Letters. 2016;171:142-145.
28. Gul I, Abbasi A, Amin F, Anis-ur-Rehman M, Maqsood A. Structural, magnetic and electrical properties of Co 1− xZnxFe 2 O 4 synthesized by co-precipitation method. Journal of Magnetism and Magnetic Materials. 2007;311(2):494-499.
29. Sattar A, El-Sayed H, El-Shokrofy K, El-Tabey M. Study of the dc resistivity and thermoelectric power in Mn-substituted Ni–

Zn ferrites. Journal of Materials Science. 2007;42(1):149-155.
30. Sattar A, El-Sayed H, Agami W, Ghani A. Magnetic properties and electrical resistivity of Zr4+ substituted Li-Zn Ferrite. Am J Appl Sci. 2007;4(2):89-93.
31. Zaki H, Mansour S. The influence of Ge 4+ and Ti 4+ ions substitution on the magnetic properties of copper ferrite. Materials Chemistry and Physics. 2004;88(2):326-332.
32. Topkaya R, Baykal A, Demir A. Yafet–Kittel-type magnetic order in Zn-substituted cobalt ferrite nanoparticles with uniaxial anisotropy. Journal of Nanoparticle Research. 2013;15(1):1-18.
33. Globus A, Pascard H, Cagan V. Distance between magnetic ions and fundamental properties in ferrites. Le Journal de Physique Colloques. 1977;38(C1):C1-163-C161-168.
34. Ashiq MN, Saleem S, Malana MA. Physical, electrical and magnetic properties of nanocrystalline Zr–Ni doped Mn-ferrite synthesized by the co-precipitation method. Journal of Alloys and Compounds. 2009;486(1):640-644.
35. Yahya N, Aripin MN, Salwani A, A Aziz A, Daud H, Mohd Zaid H, Lim KP, Maarof N. Synthesis and charaterization of magnesium zinc ferrites as electromagnetic source. American Journal of Engineering and Applied Sciences. 2008;1(1):54-57.
36. Mazen S, Dawoud H. Structure and magnetic properties of Li–Cu ferrite. Physica Status Solidi (a). 1999; 172(2):275-289.

Peer-review history:
The peer review history for this paper can be accessed here:
http://sciencedomain.org/review-history/18854